Journal of Energetic Materials
Publication details, including instructions for authors and subscription information:
http://www.informaworld.com/smpp/title~content=t713770432

Reactive flow lagrange analysis in plastic bonded explosives

Gerald L. Nutt[a]; Leroy M. Erickson[a]
[a] Lawrence Livermore National Laboratory, University of California Livermore, California

To cite this Article Nutt, Gerald L. and Erickson, Leroy M.(1984) 'Reactive flow lagrange analysis in plastic bonded explosives', Journal of Energetic Materials, 2: 4, 263 — 292
To link to this Article: DOI: 10.1080/07370658408216148
URL: http://dx.doi.org/10.1080/07370658408216148

REACTIVE FLOW LAGRANGE ANALYSIS IN PLASTIC BONDED EXPLOSIVES

Gerald L. Nutt and LeRoy M. Erickson
Lawrence Livermore National Laboratory
University of California
Livermore, California 94550

ABSTRACT

A description of Lagrange gauge measurements in PBX-9404 and RX-26-AF is given. The data are used to study the progress of reaction in these explosives. The results are discussed along with the underlying theortetical assumptions. Emphasis is given to the practical problems of constructing a description of the chemical reaction from gauge data.

*Work performed under the auspices of the U.S. Department of Energy by the Lawrence Livermore National Laboratory under contract No. W-7405-ENG-48.

Journal of Energetic Materials vol. 2, 263-292

Published in 1984 by Dowden, Brodman & Devine, Inc.

I. INTRODUCTION

This report discusses a technique developed at Lawrence Livermore National Laboratory to monitor the progress of a reaction in solid explosive. The method has been extensively treated by other authors,[1,2,3] but the procedure in the present discussion most closely follows that given by Cowperthwaite (see Vantine et al. Ref. 4).

We initiate a sample of explosive with a plane shock wave. The one dimensional flow behind the shock is measured using a series of particle velocity and pressure gauges located at Lagrange position, h. With velocity-time records at different values of h we are able to construct the particle velocity surface u(h,t), in some region of the h-t plane. Similarly, a pressure surface p(h,t) can be built. Figure 1 shows a typical experimental set up for particle velocity measurements.

At a minimum two experiments are required, one for the velocity measurements and another for pressure measurements. When pressure histories are measured, the velocity gauges indicated in Fig. 1 are replaced by manganin pressure gauges and the magnetic field is removed. It is the presence of the magnetic field that prevents use of both types of gauges in a single experiment.

The gauges used in these measurements were developed by Erickson[5,6]. The velocity data in this report were collected with anodized aluminum electromagnetic gauges. We find these gauges accurate to about 1.0 percent. The pressure histories were taken from hysteresis-corrected manganin pressure gauges which are accurate to about 2.0 percent. These data are used to calculate all of the variables describing the one dimensional flow of the reacting mixture of explosive and product gases including velocity, pressure, specific volume, and specific internal energy.

With a description of the flow, and reasonable assumptions about the equations of state of the explosive and product gases, we can calculate the mass fraction of explosive products,

$$\lambda = \frac{M_p}{M_p + M_x} \qquad 0 < \lambda < 1 \qquad (1)$$

where M_p and M_x are the mass of the product and reactant respectively. We shall refer to λ as the reaction coordinate.

This program has been carried out for two well characterized solid explosives, PBX-9404, and RX-26-AF. Both materials are composed of a finely divided explosive compound held together with a small amount of plastic bonding material. PBX-9404 is composed of 94 percent HMX, 3 percent nitrocellulose and 3 percent inert binder. 2.5 percent by weight of the HMX particles are greater than 300 μm size. RX-26-AF is an experimental plastic bonded explosive (PBX). Its composition by weight is 46.6 percent TATB, 49.3 percent HMX, and 4.1 percent Estane Poly(urethene-ester-MDI) inert binder. The particle sizes in RX-26-AF are all less than 60 μm. We will show evidence that the explosive particle size has a significant effect on the gauge response.

The alternative approach of building a p(h,t) surface has been explored elsewhere. Using pressure histories from embedded gauges and a $p(V,E,\lambda)$ equation of state, reaction rates have been calculated by Wackerle, Johnson, and Halleck.[2] The assumption underlying the equation of state is the equilibration of the temperatures of explosive and product. Kanel and Dremin[3] also use a pressure surface, but assume that no heat is exchanged between reactant and product.

In the following sections we will briefly discuss the theory of reactive flow Lagrange analysis (RFLA), describe the construction of the u(h,t) surface, discuss the equations of state of reactants and products, and show the time histories of the reaction in PBX-9404 and RX-26-AF.

II. THEORY

If we can understand the development and shape of the surface u(h,t), we can easily construct the remainder of the flow variables through the one dimensional Lagrange equations for fluid motion:

$$V(h,t) = V_s + V_o \int_{t_s}^{t} \frac{\partial u}{\partial h}\, dt \tag{2}$$

$$p(h,t) = p(h',t) - \frac{1}{V_o} \int_{h'}^{h} \frac{\partial u}{\partial t} dh \tag{3}$$

$$e(h,t) = e_s - V_o \int_{t_s}^{t} p \frac{\partial u}{\partial h} dt \quad . \tag{4}$$

The subscript s refers to a shock boundary condition, and o to conditions in front of the shock wave. V is the specific volume, p the pressure, and e the specific internal energy of the reacting fluid. Calculation of the pressure requires a pressure history at some position $h = h'$ covered by the surface $u(h,t)$. Clearly, it is necessary that the measurement of the flow velocity be precise enough to supply accurate partial derivatives of u with respect to h and t.

It is believed that a reaction starting in explosive material begins at certain reaction sites called "hot spots" and that a laminar combustion wave proceeds from these sites subsonically, to consume the entire explosive. This generalization of the well known ZND (Zeldovich, von Neumann, Doering) model of detonation can be expressed as a pressure equilibrium between the explosive and product gases

$$p(h,t) = p^x(h,t) = p^p(h,t). \tag{5}$$

The superscripts x, and p refer to the explosive and product respectively.

The boundary between the explosive and product is formed by the thin combustion wave. Although the wave is characterized by high temperatures (2000-3000 K), we will assume that low heat conductivity prevents significant transfer of heat from the front into the explosive on a time scale comparable to characteristic reaction times. The effect of this assumption is that the entropy is constant in the unreacted explosive phase of the mixture during the reaction. The entropy production occurs only in the thin reacting burn front.

The internal energy and specific volume obey

$$e(p,V,\lambda) = \lambda e^p(p,V^p) + (1-\lambda)e^x(p,V^x), \text{ and} \tag{6}$$

$$V = \lambda V^p + (1-\lambda)V^x \quad . \tag{7}$$

using Eqs. (2) and (4) to evaluate the left hand sides of Eqs. (6) and (7) respectively, and using the isentrope for the explosive to determine V^x, we obtain two equations with the unknowns λ, and V^p. Consequently, all the

flow variables can be obtained if we are able to supply the equations of state for the explosive and product gases. These equations of state have been determined for the JWL[7] form:

$$p = A\left(1 - \frac{\omega V_o}{R_1 V}\right) \exp(-R_1 V/V_o) + B\left(1 - \frac{\omega V_o}{R_2 V}\right) \exp(-R_2 V/V_o) + \frac{\omega e}{V} \quad . \qquad (8)$$

The isentrope for this equation of state is:

$$p = A \exp(-R_1 V/V_o) + B \exp(-R_2 V/V_o) + C\left(\frac{V}{V_o}\right)^{-\omega - 1} \quad . \qquad (9)$$

The constants in these equations have been fixed for the product gases by cylinder test data and Chapman-Jouguet (C-J) measurements which define the release isentrope. For the explosive, the constants are fixed by a fit to a very limited amount of Hugoniot data. The constants appropriate for PBX-9404 and RX-26-AF are shown in Table 1.

The difference between the specific internal energies of the reactant and product gases at standard conditions is the quantity Q given in Table 1:

$$Q = e_o^x - e_o^p \quad , \qquad (10)$$

which defines the relative energy scales of the JWL equations for explosive and product.

Using this result in Eqs. (4) and (6) yields

$$\frac{1}{2} p_s (V_o - V_s) - V_o \int_{t_s}^{t} p \frac{\partial u}{\partial h} \, dt = \lambda (e^p - Q) + (1 - \lambda) e^x \quad . \qquad (11)$$

V^x can be calculated from Eq. (9) by substituting V^x for V, and using the appropriate constants for the reactant from Table 1. Notice that the constant C in Eq. (9) is a function of entropy only and is determined by conditions at the shock front.

In summary, the reactant and product equations of state, along with u(h,t) and a single pressure history p(h',t), close the equations of motion and allow us to calculate $\lambda(h,t)$.

III. THE LAGRANGE GAUGE MEASUREMENTS

Our experimental samples of explosive (see Fig. 1) are right circular cylinders 16 mm high and 90 mm in diameter. The gauges are placed near the axis at various distances h, from the base. A plane shock wave is generated by a cylindrical Kel-F flyer hitting a Kel-F buffer at a velocity of 0.86 mm/μs. The resulting symmetrical impact creates a shock which is transmitted through the buffer to the HE. The arrival of the shock at the HE surface is registered by a pressure or velocity gauge establishing the time base for the Lagrange Analysis. The pressure at this surface is sustained through the experiment, and the data are gathered before lateral relief waves can affect the gauge readings. The input pressure is nominally 2.5 GPa.

Figure 2 shows a typical collection of velocity, and pressure histories. The analysis is performed around the pressure curve bracketed by three velocity-time curves.

The velocity gauge signal is a voltage-time curve photographically recorded from an oscilloscope trace. The pressure gauge output is a resistance-time curve similarly recorded by an oscilloscope. These traces are compared with the gauge calibration data and directly converted to velocity and pressure histories. The data is then digitized and a cubic spline fit is generated using nine knots. Typically, the fits are generated using approximately 100± 10 points. The knots are adjusted until the scatter about the spline is less than ±2.0 percent for the velocity, and about ±5.0 percent for the pressure data respectively.

The use of nine knots (eight spline segments) was arrived at as a compromise between good resolution of the digitized data, by which we mean small scatter about the fit, and resolution of the noise in the data. By increasing the number of spline segments to fit, for example, one hundred points, we can make the scatter about the spline arbitrarily small. Unfortunately, in the limit of twenty-five spline segments we get a curve with wildly changing derivatives destroying the usefulness of the spline. To some extent this choice involved judgements as to what are the physical features of the data and what is "noise." Such judgements are aided by comparison with many nearby measurements, reproducibility, and the requirement that the surface be a smooth function of h as well as t.

It is necessary, if we are to construct a surface out of the curves, that each u-t curve have the same number of spline segments and that there be a correspondence between the knots (or end points of a spline segment) on a particular curve with the knots on the neighboring curve. Thus, starting from the first knot at the shock, the third knot always lies on the first maximum, the sixth knot lies at the minimum. The eight and ninth knots mark the second peak (if any) and the end of the data respectively.

The next step is to subdivide each spline segment of the three particle velocity curves into ten segments. The corresponding division points in each of the three records are then jointed by a second degree spline. Thus, we are able to construct the u(h,t) surface using a dense set of points and we can calculate all the first derivatives of the surface at these points.

Returning to Fig. 2, with increasing h we notice an increase in the maximum velocity, indicating the reaction is building toward detonation. At h = 10 mm we see a definite minimum in the velocity time curves, and the beginning of a second maximum. At h = 13 mm the second maximum is clearly evident. This minimum must be associated with a maximum in the pressure vs. h curve as required by the momentum equation. The second velocity maximum, however, is not as easy to interpret; does it arise from the rarefaction originating from the rear of the sample, or does it indicate further reaction in the explosive? It is important to notice that the data in Fig. 2 are taken from RX-26-AF samples with fast burning (HMX) and slow burning (TATB) components. The second maximum appears also in the PBX-9404 data but it is not as pronounced as in RX-26-AF. The velocity time curves for these two explosives taken at h = 10 mm from the front of the sample are shown in Fig. 3 for comparison.

We studied this problem using the DYNA2D computer code to model the experiments. Reactive flow models for the two explosives were used.[8,9] The calculations were done with the rear surface of the explosive terminated with teflon at h = 16 mm, as in the experiments, and also with the teflon replaced by more HE.

For PBX-9404, the calculation showed a second maximum in the velocity just as in the experiment. With teflon replaced by explosive, the second maximum disappeared. When we changed the reactive flow model to one

representing RX-26-AF we found a much larger second maximum in the u-t plots. The second maximum was reduced, but did not disappear, when explosive replaced the teflon. Our conclusion is that for PBX-9404, the second maximum is not associated with the chemistry. For the analysis of RX-26-AF the second maximum cannot be ignored. As a result we thought it prudent to include the second maxima in our fits to the u-t curves for both explosives.

The pressure time data presented another puzzle. It is normal practice in these experiments to use two, and sometimes four, gauge foils at a given Lagrange position. Figure 4 gives a sample of the comparison between pressure histories of the two explosives and also between a pair of records in each explosive at the same Lagrange station (h = 6 mm).

In the RX-26-AF, each pressure gauge agrees with its neighbor at the same Lagrange station to within a few percent. In the PBX-9404 on the other hand, the neighboring gauges agree only when the pressure is increasing and disagree strongly when pressure decreases with time as shown in Fig. 4. In each of the explosives there are at least six such pairs of pressure records and we found no exceptions to this rule.

In the PBX-9404 we are clearly observing a significant departure from our theoretical model of a homogeneous reacting fluid. Figure 4, and the foil separation, indicate pressure gradients of the order of 50 kbar/mm. These inhomogeneities are apparent only in the later stages of the reaction when the rate of pressure increase due to the reaction is nearly balanced by the pressure decreases due to expansion. Such inhomogeneous reaction apparently does not occur in RX-26-AF.

It is interesting to note that the specifications for the explosives differ in the allowable explosive particle size used for their manufacture. The PBX-9404 calls for 75 percent of the HMX particles to be greater than 0.16 mm while the particle sizes in RX-26-AF are not greater than 0.06 mm. Inspection of the surface of HE samples by microscope shows rather large crystals of HMX (about 0.5 mm) with separations on the order of 1.0 mm. Such large crystals are not present in the RX-26-AF.

This evidence suggests the inhomogeneities observed by the pressure histories in PBX-9404 are related to the burning of the large crystals during the late stage of the reaction. Probably, the smaller particles are consumed

early in the reaction and the large particles dominate as the reaction completes. The characteristic gauge active element is a 0.7 mm x 2.0 mm rectangle, while the gauge separation is several millimeters, or about the same distance as the separation of large HMX crystals. We believe disagreement between neighboring gauges does not occur in RX-26-AF because the large explosive crystals are not present.

Assuming a sound speed of approximately 6 mm/μs in the PBX-9404 products, it is not credible that a pressure difference on the order of 10 GPa can be maintained for a full microsecond over the few millimeters separating the two gauges. Such a pressure gradient would destroy the gauges. Yet, the current in each gauge is constant for some time after they begin reporting difference pressures. The best explanation we can offer for the presistence of disagreement in gauge signals, is that the local pressure fluctuations perforate the Teflon armor opening a shunt current path in the gauge leads. This would cause a lowering of the pressure signal. The problem is not a serious one for RFLA since it affects only the very end of the reaction. In any case, we always do the analysis using the higher pressure reading.

Our experience shows the most troublesome source of error in RFLA is the reproducibility of the flyer velocity. At least two experiments are necessary to complete the analysis: one to map out the $u(h,t)$ surface, the other to provide a pressure history for the initial condition in Eq. (3). The pressure at the shock front is determined by the shock trajectory $h(t)$, and the particle velocity, both given by the velocity gauge measurements.

$$p_s = \frac{u_s}{V_o} \frac{dh(t)}{dt} \tag{12}$$

The same pressure is also determined independently with the pressure gauge measurements. Unless the flyer velocity is exactly the same in both experiments these shock pressure determinations will not agree.

The effect shows up when h, the Lagrange coordinate of the calculated pressure is smaller than h', the position of the pressure gauge. Figure 5 shows the region of the h-t plane in the neighborhood of the pressure gauge record. For $h' > h$ we must divide the integration into two regions. One region uses the gauge measurement as the initial condition. This region is indicated in Fig. 5 by the bracket labeled 2. The other region, indicated by

the bracket labeled 1, uses Eq. (12) where the right hand side is evaluated entirely from velocity gauge data. This situation can lead to a discontinuity in the calculated pressure history at h.

We deal with this problem by scaling the pressure measurement by a constant factor to agree with Eq. (12). The consistency of different data sets is judged by the closeness of the scaling factor to unity.

A one percent difference in flyer velocity will affect the particle velocity at the shock front by about a percent. The coresponding pressure will be affected by approximately 2 percent, and because of the pressure dependence of the reaction rate we can expect a cumulative effect later in the flow.

Variations in flyer velocity amplify differences in particle velocity deep in the flow. This causes even greater fluctuations in the gradients of the velocity surface. Consequently, it is extremely difficult although not impossible to create the surface from velocity histories when all the velocity records are not from the same experiment.

IV. RESULTS

A. PBX-9404

Out of thirteen experiments with PBX-9404 we have selected a single particle velocity experiment spanning the region 3 mm < h < 7 mm. The three velocity time records are denoted 3919G, K, and N. Two pressure experiments are chosen to complete the data: 3911K located at h = 3.98 mm, and 3910K located at h = 6.046 mm. These pressure shots were selected because of their location and because of their consistency with the velocity data. Pressure record 3910K only needed a -2.4 percent adjustment to agree with experiment 3919, and the pressure gauge 3911K only needed +0.5 percent adjustment. According to the velocity data, the shock pressure is 2.38 GPa, and 2.50 GPa at h = 3.98 mm, and 6.046 mm respectively.

The results for PBX-9404 are displayed in Fig. 6a and b showing the reaction coordinate λ and the reaction rate $d\lambda/dt$ respectively, at h = 3, 4, 5, 6, and 7 mm. Each curve has two traces superimposing results from the two pressure shots. The consistency is obviously good.

The reaction coordinate, λ, follows the expected s-shaped curve but does not reach the value 1.0 for Lagrange coordinates $h < 5$ mm during the time spanned by our measurements. The reaction rate shows a single peak except for the one located at 3 mm in shot 3911K. The double peak appears occasionally at small values of h.

The reaction rate curves agree better on the upslope than on the downslope. This is expected from our discussion of the poor agreement between different pressure gauge measurements in PBX-9404 which always diverge as the reaction goes to completion. The reaction indicates termination at a slightly larger value of λ when the RFLA is performed with pressure record 3911K, and the peak reaction rates are higher when using 3910K.

We attribute the difference in maximum values of λ computed with the two pressure records, primarily to the degree to which they are consistent with the velocity measurements. Thus, λ computed using 3911K, which only required a 0.5 percent adjustment to fit the velocity data at the shock front gives a maximum value of λ of 0.880 at $h = 4.0$ mm while 3910K, requiring a 2.4 percent adjustment gives a maximum of 0.750. Similarly, at $h = 6.0$ mm 3911K and 3910K give maximum λ of 0.916 and 0.803 respectively.

B. RX-26-AF

Nine experiments were performed with RX-26-AF. Of these we select two particle velocity experiments to construct the velocity surface. Measurements 3915E, H, and L provide the data in the region $3.0 \text{ mm} < h < 7.0$ mm. Pressure gauge 3822H, located at 6 mm, provides the pressure data which agree with 3915 velocity data to 0.09 percent. Particle velocity measurements were also taken from experiment 3821 to extend the analysis to values of h less than 3 mm and beyond 7 mm. Whatever combination of velocity data was used, the agreement between pressure and velocity data was within 1.25 percent at the shock front with a pressure of 2.46 GPa.

The composite analysis results are shown in Figs. 7a and b. The reaction takes about 6 μs to complete as compared with 3.5 μs for PBX-9404 with the same input shock pressure. The reaction rate shows two maxima rather than the single sharp maximum found in PBX-9404. We believe this shows two distinct reactions in the RX-26-AF. As the reaction builds for larger values of h, the two rates grow and appear to separate.

These results strongly suggest that HMX and TATB follow their own separate reactions: the HMX burns quickly, raising the pressure above about 8.0 GPa, followed by the reaction in TATB. The two large and separate reactions appearing at h = 8, and 9 mm is graphic support for this conjecture. These results are also consistent with our experience that approximately 7.5 GPa is the lowest input pressure that will shock initiate TATB.

Figures 6 and 7 show maximum values of λ somewhat less than 1.0 apparently indicating the reaction does not run to completion in these experiments. Some sets of data show λ reaching a maximum, $\lambda_{max} > 1.0$ which is physically unreasonable. Such data, however, do not have good consistency between the velocity and pressure measurements, requiring an adjustment of 7 to 8 percent in the pressure. Generally, our results lie in the range λ_{max} 1.0 ± 0.1, but the best data gives λ_{max} about 0.9.

We conclude that for both explosives, error in measurement propagates through the analysis to an uncertainity of ten percent in λ. Our data seem to be biased toward the low values of λ. This suggests that the accuracy of the equation of state parameters in Table 1, determined near the C-J point, is impared when the shock initiation pressure is an order of magnitude lower. Thus, the product equation of state may be providing a systematic error. Our best results with PBX-9404 suggests the error is somewhat less than ten percent.

V. DISCUSSION

An interesting feature of the reaction growth is the delay between shock arrival and the actual increase in λ. The delay is generally more than 1.0 μs during which time λ takes on slightly negative values. This is not physical unless one can postulate some endothermic process occurring before the transformation of explosive into product gases.[10] We believe negative λ is a manifestation of the visco-plastic work done on the explosive in compressing the initiation sites, leading to formation of hot spots. Although the accuracy of our analysis is not sufficient to claim we are measuring the energy going into hot spot formation, this conjecture is supported by the persistent occurrence of small negative values of λ calculated with nearly all the data and by the reaction delay which is comparable with the time of visco-plastic pore collapse.[11]

Referring to Fig. 4, we have hatched the part of the pressure history corresponding to reaction growth. The reaction always terminates at a point

occurring slightly later than the maximum in pressure. This is to be expected. Assuming no heat conduction through the boundaries of the reacting fluid we have.

$$\frac{\partial e}{\partial t} = -p \frac{\partial V}{\partial t} \quad , \tag{13}$$

where the time derivatives are Lagrangian. Using Eqs. (6) and (7), and restricting the state of the explosive (but not the product gases) to an isentrope allows us to express e as a function of p, V, λ, and the specific entropy of the explosive, s^x. As a result, Eq. (13) can be put in the form

$$\frac{\partial p}{\partial t} = -\left(\frac{c}{V}\right)^2 \frac{\partial V}{\partial t} - \left(\frac{\partial e}{\partial \lambda}\right)\left(\frac{\partial e}{\partial p}\right)^{-1} \frac{\partial \lambda}{\partial t} \quad . \tag{14}$$

The sound speed c in the reacting mixture is given by

$$\frac{c^2}{V^2} = \left(p + \frac{\partial e}{\partial V}\right)\left(\frac{\partial e}{\partial p}\right)^{-1} \quad . \tag{15}$$

The partial derivatives of $e(p,V,\lambda,s^x)$ appearing in Eqs. (14) and (15) are to be taken with p, V, λ, s^x constant (except for the independent variable actually appearing in the derivative). It can be shown that $\partial e/\partial \lambda$ in Eq. (14) is negative, so the rate of change in pressure due to the progress of the reaction is positive.

Equation (14) is a statement that fluid pressure change is a competition between growth due to reaction, and decrease due to expansion. When $\partial \lambda/\partial t = 0$ in Eq. (14), $\partial p/\partial t < 0$. Our results are always consistent with this condition.

Within the limits of our simplifying thermodynamic assumptions we can explore the state of the reactive flow in fine detail. Figures 8 and 9 show the state path of a particle located at h = 6 mm in both explosives. Figure 8 is a three dimensional plot of the path of a particle of PBX-9404 from shock arrival to reaction termination. The path begins by departing from the reactant isentrope. Following a short initiation process the particle follows a trajectory intersecting the product isentrope tangentially.

In Figs. 8 and 9 only a short segment of the product isentrope is displayed, joined to a segment of the state path of the products.

The analysis shown in Fig. 8 was selected because the reaction terminated with a value $\lambda_{max} = 1.0$. It is this property which allows the state path to intersect the product isentrope. For clarity on this point, Fig. 9 shows a similar state path in RX-26-AF where $\lambda_{max} = 0.834$. The state path is separated from the product isentrope at the end of reaction.

The experiments shown in Figs. 8 and 9 are far from steady state detonations. However, it is interesting to compare the results with the ZND[12] model of detonation. Briefly, the ZND model describes detonation as a shock in the reactant, preceeding a C-J deflagration. The deflagration is centered at the shock and proceeds down a Rayleigh line in the p-V plane to a point of simultaneous tangency with the product isentrope and Hugoniot. The two segments of the Rayleigh line, going from the initial state and the shock state, and from the shock to the C-J point are colinear in a steady detonation wave.

Figure 10 shows what happens in the unsteady wave building to detonation. It is what one sees in Fig. 8 by viewing along the e-axis. The interpretation of Fig. 10 is aided by referring to Eq. (14).

The shock arrives at the fluid sample at $t = 1.78\ \mu s$. At first $d\lambda/dt$ is small while the fluid is compressed in the neighborhood of the explosive isentrope. As reaction builds, we reach a point of maximum compression where $dV/dt = 0$ and the increase in pressure is entirely due to the growth of the reaction. This point is marked $t = 2.77\ \mu s$. A microsecond later the pressure is at a maximum. In Eq. (14) this point corresponds to a balance between the terms representing expansion of the fluid and reaction progress. At $t = 4.19\ \mu s$, λ reaches its maximum value and the state point joins the product isentrope.

If we imagine this process building to steady detonation the state path will collapse to a straight line. The points of maximum compression and maximum pressure will coincide. Thus, the pressure maximum will not be a von Neumann spike at the shock front unless dV/dt and $d\lambda/dt$ vanish there simultaneously. It may, in fact, lie at a point near the end of the reaction. This separation of pressure maximum from shock arrival has been reported independently in the case of full running detonations.[13]

VI. CONCLUSION

We have demonstrated the usefulness of RFLA in studying the shock initiation of two important solid explosives with very different burn characteristics. We have resolved the entire reaction process. As a result we are able to get a picture of the process of initiation as well as the growth of reaction. The clear separation of HMX and TATB rates in Fig. 7b shows the utility of RFLA in evaluating the performance of explosives mixtures. Studies of the effect of finely divided fuels and oxidizers may be possible if the oxidation reaction is not delayed so long that the gauges fail before the end of reaction.

The overall reported accuracy of these results is certainly adequate to resolve interesting features of the reaction process. The main limitation on accuracy at this point is reproducibility of the flyer velocity from the particle velocity to the pressure experiments. We expect to have greater control over this in future experiments. Because the reaction time is shorter as the reaction grows, we will need better time resolution in the experiments to carry out RFLA closer to detonation. Present time resolution does not permit sufficiently accurate fits to the time history curves to allow us to analyze shock runs greater than 10.0 mm. In fact, for $h > 8.0$ mm the results are very difficult to obtain.

There is a clear application of RFLA in investigating the reaction rate equations for use in computer models of high explosive burn. These rate equations have a number of terms whose importance is a matter of speculation. The reactive flow model can be compared directly with Figs. 6 and 7.

We have only been able to analyze the interesting shock initiation properties of TATB through our experiments with RX-26-AF. The reason for this is due to limitation on the flyer velocity in our present gun system which restricts our initiation pressures to less than 9.0 GPa. TATB, however, requires sustained pressures in excess to 11.5 GPa for reliable, homogeneous initiation. We hope to solve this problem soon with new high density non-metallic flyer material which will permit a direct RFLA to be performed on a plastic bonded, TATB based, explosive.

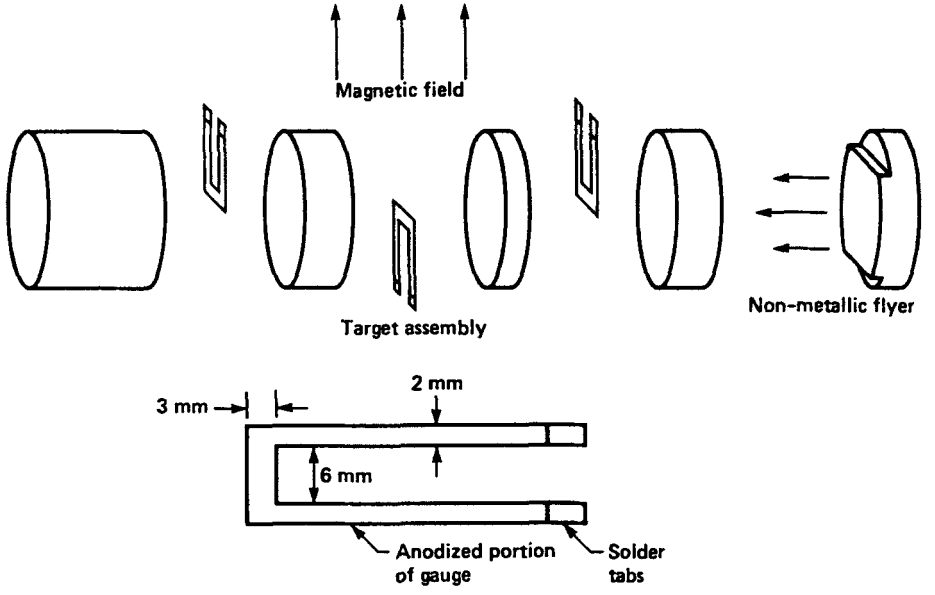

Fig. 1 Exploded view of a typical multiple gauge installation showing gauge orientation. Flat edges on flyer are provided to minimize lead spreading effects from edge rarefaction. Dimensional details of the gauge are shown in the sketch at the bottom of the figure.

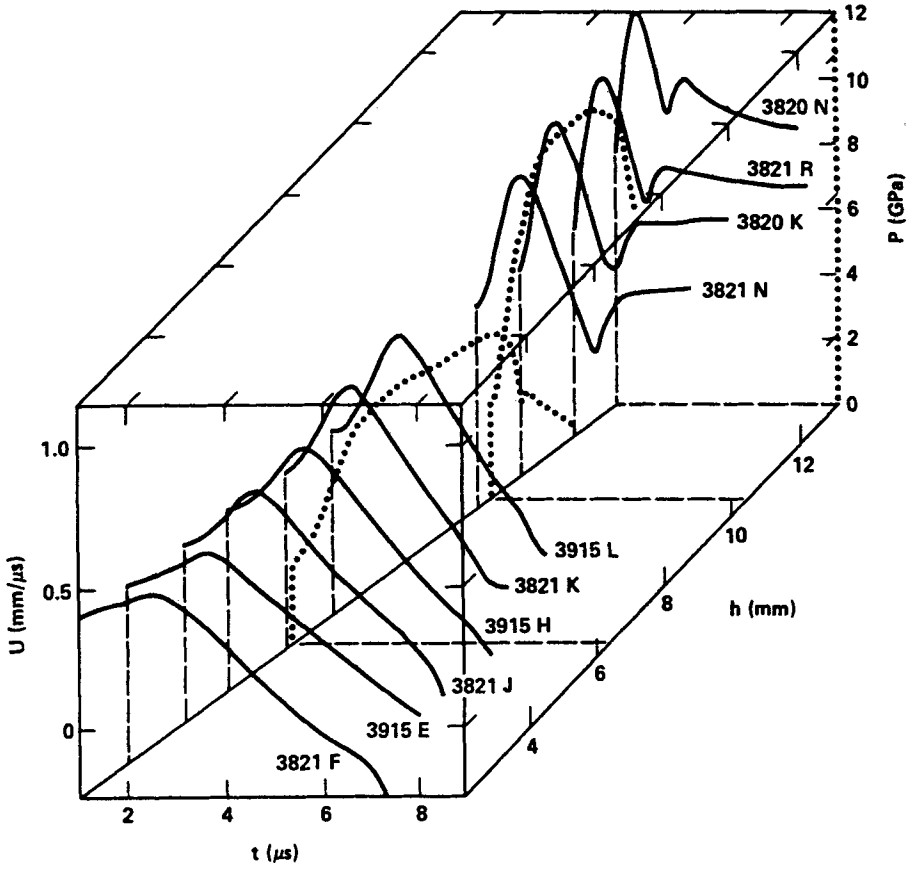

Fig. 2 A typical collection of velocity time records from several different experiments. Three are selected to form the U(h,t) surface. Also shown are two pressure records which are used in the integration of the equations of fluid motion. These data are taken from experiments with RX-26-AF.

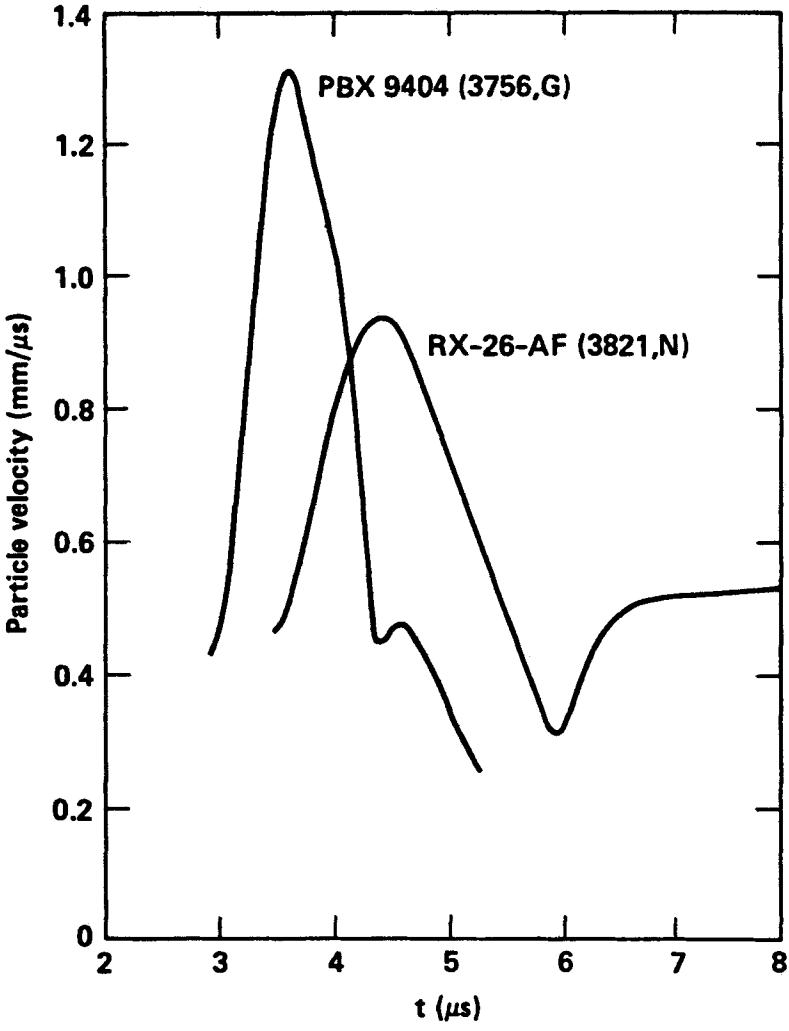

Fig. 3 Comparison of velocity records at h = 10 mm. Note the relative size of the second increase in velocity in the two explosives.

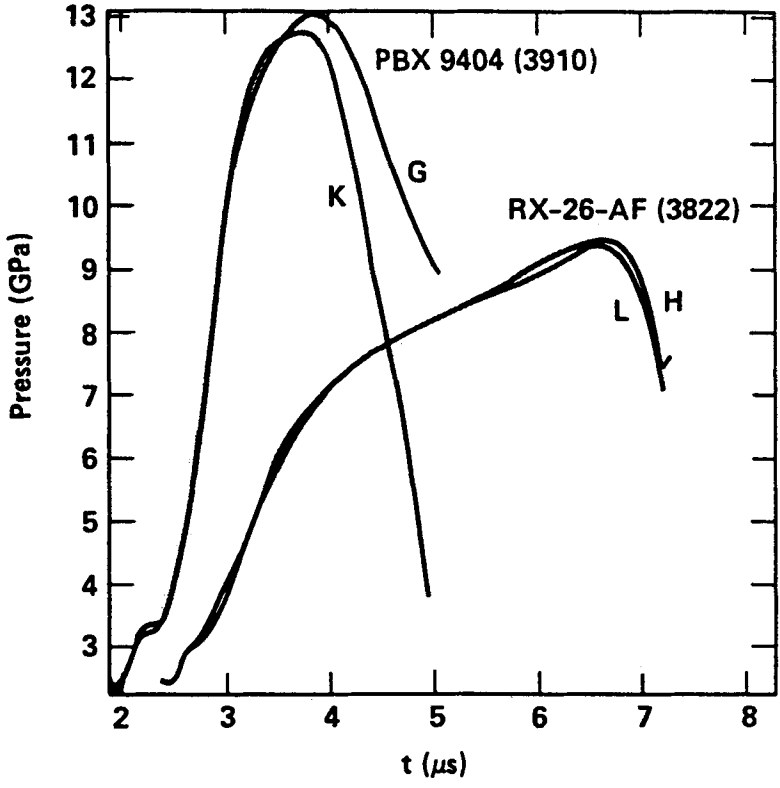

Fig. 4 Comparison of typical pressure record data in RX-26-AF and PBX-9404. Each explosive has two pressure gauges h = 6 mm. The agreement between two measurements in RX-26-AF contrasts with strong disagreement between gauges in PBX-9404. The shaded bands indicate the times when λ is increasing from a value of 0.0.

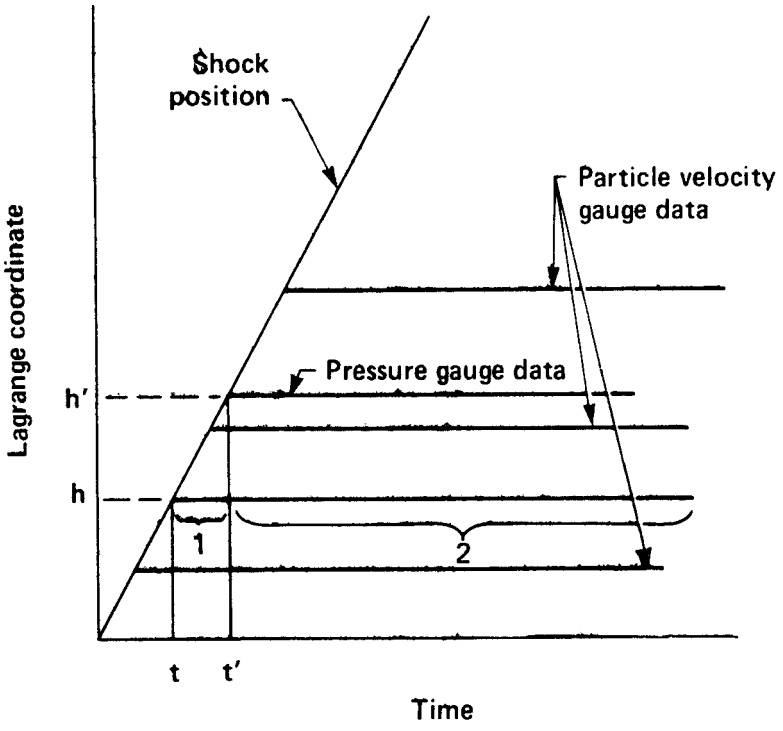

Fig. 5 Diagram of regions of integration in the h-t plane required for Eq. (3). If $h < h'$ the initial condition must be taken from the shock trajectory in region 1, and from the pressure gauge measurements in region 2.

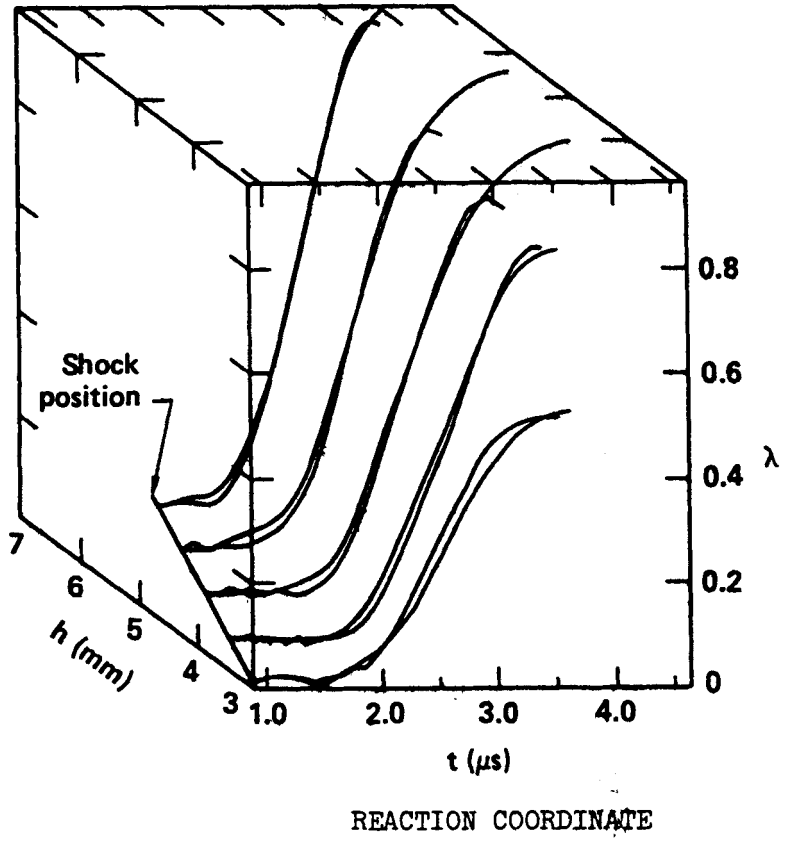

Fig. 6a Analysis in shock initiated PBX-9404 using velocity measurements 3919G, K, N. The pressure measurements are 3911K, and 3910K. Maximum λ is always greater when 3911K is used than with 3911K.

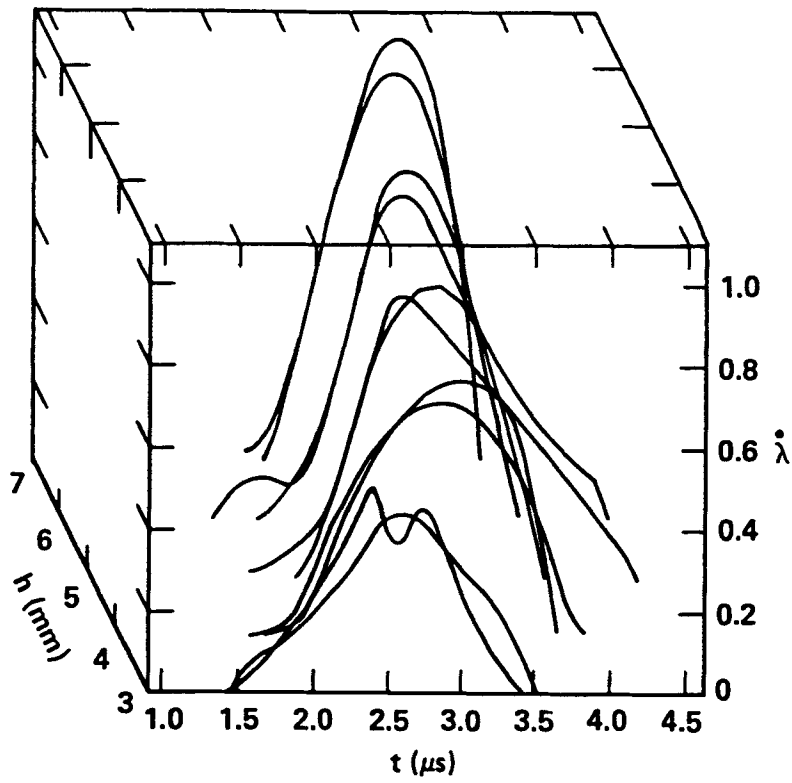

Fig. 6b Analysis in shock initiated PBX-9404 using velocity measurements 3919G, K. N. The pressure measurements are 3911K, and 3910K. Maximum λ is always greater when 3911K is used than with 3911K.

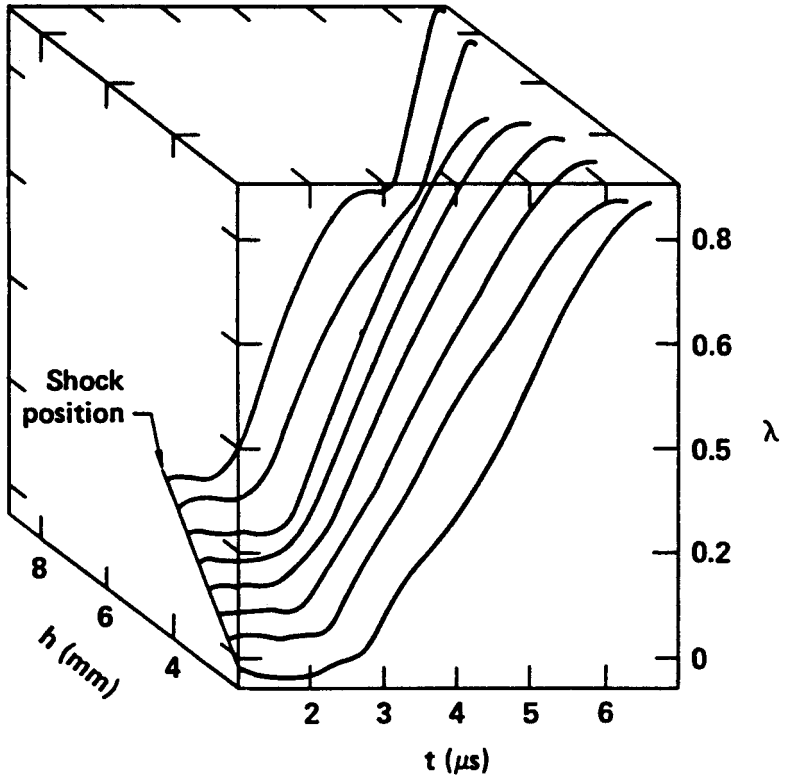

Fig. 7a Analysis in shock initiated RX-26-AF using velocity gauges 3915E, H, L, and pressure gauge 3822H.

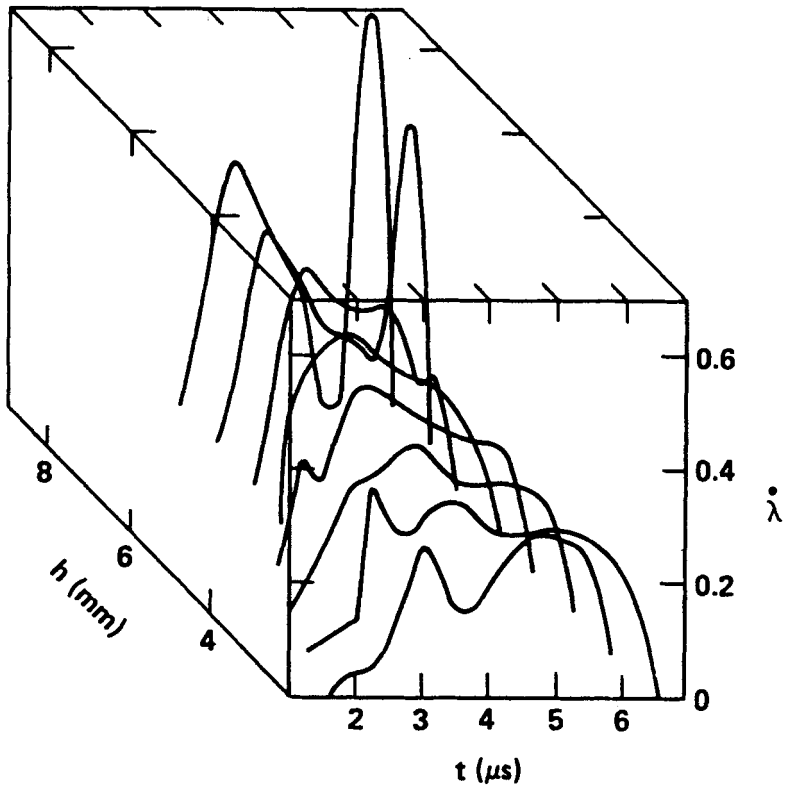

REACTION RATE

Fig. 7b Analysis in shock initiated RX-26-AF using velocity gauges 2915E, H, L, and pressure gague 3822H.

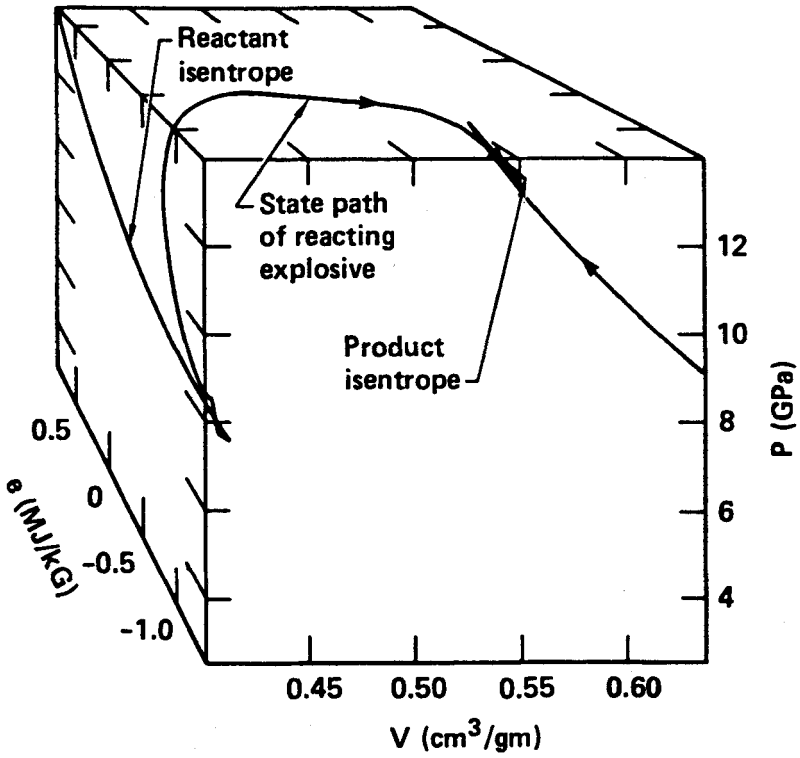

Fig. 8 State path of reacting PBX-9404. The reaction begins as the system leaves the isentrope of the explosive and terminates on the product isentrope. RFLA data are from velocity measurements 3919G,K, N and pressure measurement 3910G.

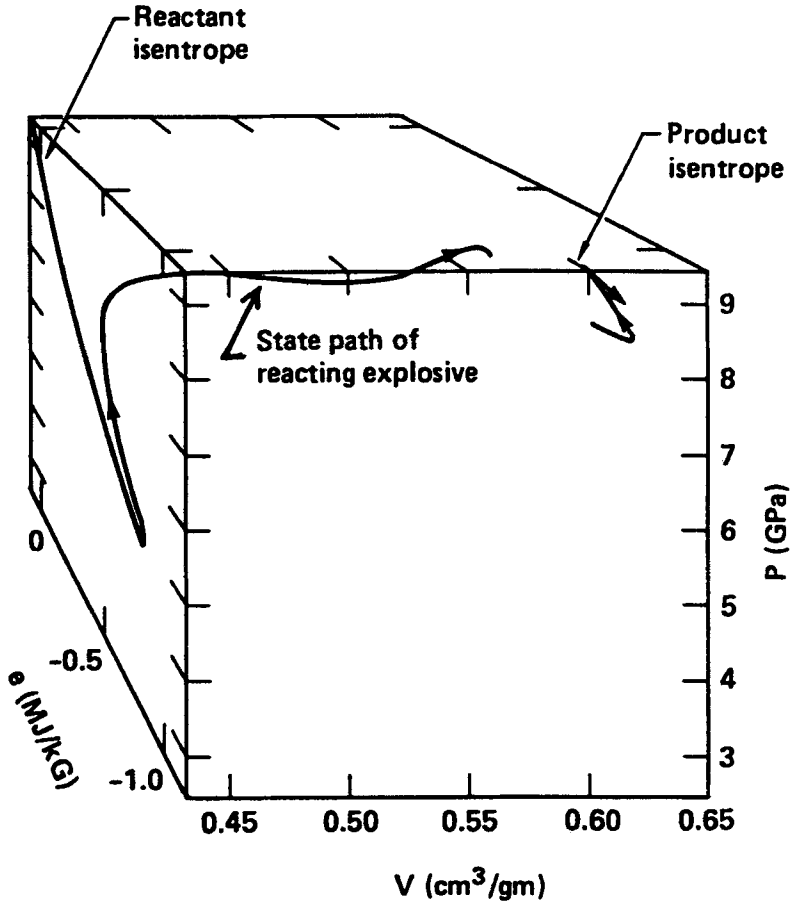

Fig. 9 State path of reacting RX-26-AF. State path does not interect product isentrope because $\lambda_{max} \neq 1$. RFLA data are from experiments 3915E, H, L, and 3822H.

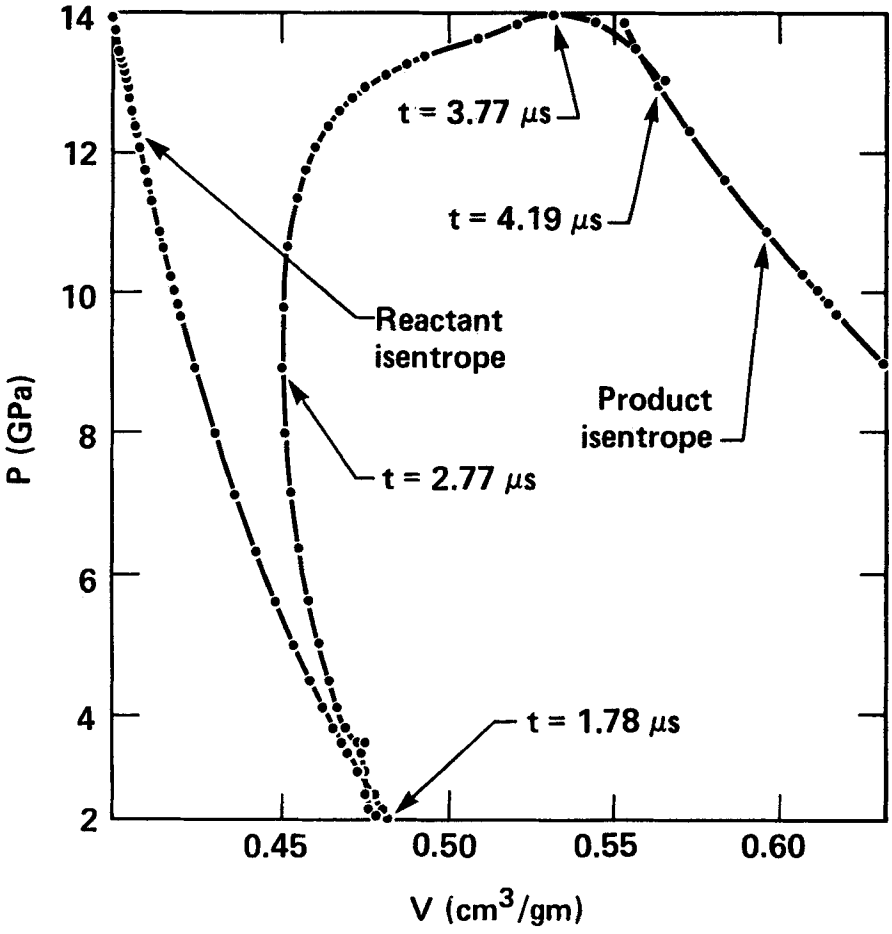

Figure 10. State path of PBX 9404 in PV-plane. Projection of Figure 8 along e-axis. Dots indicate points calculated by RFLA.

ACKNOWLEDGMENT

The authors acknowledge with thanks the help of Robert Rainsberger of Lawrence Livermore National Laboratory, whose expert programming made the computer code "RFLA" a powerful tool for Lagrange Analysis. Also, Michael Cowperthwaite of SRI International for many helpful discussions.

We are especially grateful to Frederick N. Fritsch for showing us how to handle a difficult convergence problem in our numerical solution for λ.

REFERENCES

1. M. Cowperthwaite, "Determination of Energy Release Rate with the Hydrodynamic Properties of Detonation Waves," 14th Symposium (International) on Combustion, (The Combustion Institute, Pittsburgh), 1259, 1973.
2. J. Wackerle, J. O. Johnson, P. M. Halleck, "Shock Initiation of High Density PETN," 6th Symposium (International) on Detonation, Office of Naval Research, Washington, 20, 1976.
3. G. L. Kanel and A. N. Dremin, "Decomposition of Cast Trotyl in Shock Waves," Combustion, Explosion and Shock Waves, 13(1), 71 (1977).
4. H. C. Vantine, R. B. Rainsberger, W. D. Curtis, R. S. Lee, M. Cowperthwaite, J. T. Rosenberg, "The Accuracy of Reaction Rates Inferred from Lagrange Analysis and In Situ Gauge Measurements, " 7th Symposium (International) on Detonation, 466, (1981).
5. L. M. Erickson, C. B. Johnson, N. L. Parker, H. C. Vantine, R. C. Weingart, "The Electromagnetic Velocity Gauge: Use of Multiple Gauges, Time Response, and Flow Perturbation," 7th Symposium (International) on Detonation, 1062, (1981).
6. H. C. Vantine, L. M. Erickson, J. A. Janzen, "Hysteresis-Corrected Calibration of Manganin Under Shock Loading," J. App. Phys. 51, 1957 (1980).
7. E. L. Lee, H. C. Hornig, J. W. Kury, "Adiabatic Expansion of High Explosive Detonation Products," UCRL-50422, Lawrence Livermore National Laboratory, (1968).
8. J. O. Hallquist, "Users Manual for DYNA2D - An Explicit Two-Dimensional Hydrodynamic Finite Element Code With Interactive Rezoning," Lawrence Livermore National Laboratory, UCID 18756, Rev. 1 (1982).
9. E. L. Lee, C. M. Tarver, "Phenomenological Model of Shock Initiation in Heterogeneous Explosives," Phys. Fluids, 23, 2362, (1980).
10. C. M Tarver, "Chemical Energy Release in One-Dimensional Detonation Waves in Gaseous Explosives," Comb. Flame, 46, 111 (1982).
11. B.A. Khasainov, A.A. Borisov, B.S. Ermolaev, A.I. Korotkov, "Two-Phase Visco-Plastic Model of Shock Initiation of Detonation in High Density Pressed Explosives," 7th Symposium (International) on Detonation, 435, (1981).
12. J. von Neumann, "Theory of Detonation Waves," In John von Neumann, Collected Works. Vol. 6, A.J. Taub ed., MacMillan, New York.
13. B. Hayes, private communication.

TABLE 1

Jones-Wilkins-Lee (JWL) Equation of State Parameters

	GPa A(GPa)	GPa B(GPa)	R_1	R_2	W	Q(MJ/kg)
PBX-9404:						
Reactant	6969.	-172.7	7.8	3.9	.858	
Products	852.4	18.02	4.6	1.3	.38	5.56
RX-26-AF:						
Reactant	201100.	-5.204	12.4	1.24	.945	
Products	801.8	52.64	5.0	2.1	.34	4.64